Kinetic Study of Vapor-Phase Preparation of Orthorhombic Molybdenum Trioxide

H. C. Zeng,* C. W. Sheu, and H. C. Hia

Department of Chemical Engineering, Faculty of Engineering, National University of Singapore, 10 Kent Ridge Crescent, Singapore 119260

Received May 8, 1997. Revised Manuscript Received December 29, 1997

A new kinetic approach to study the vapor-phase preparation of orthorhombic molybdenum trioxide (MoO_3) has been established in this work. Using a simple experimental setup, the vaporization and condensation of MoO_3 can be investigated with sufficient oxygen background to ensure the stoichiometry of the compound. The empirical condensation rate of the MoO_3 obtained in the temperature range 642−660 °C is $R_E = 1.20 \times 10^{-3}\Delta P^{2.07}$, where ΔP is the partial pressure difference of MoO_3 between the source and condensed crystals. On the basis of the observed crystal morphology and XRD results, a more precise MoO_3 condensation kinetic model has been developed to explain the layer-by-layer growth of orthorhombic structure. The staged growth phenomena can be interpreted by this mechanistic model, which correlates the condensed MoO_3 weight data to the experimental setup. The driving force of the condensation growth is investigated with respect to the current experimental conditions. For the MoO_3 partial pressure ratios of 3.86−2.97 between the source and condensed MoO_3, free energy changes determined for the growth are in the range −10.7 to −8.8 kJ/mol.

Introduction

In recent years, molybdenum trioxide (MoO_3) derived materials have received increasing attention due to their important applications as charge-density wave conductors,[1,2] optical materials,[3−5] display devices,[6,7] and catalysts.[8−11] In the area of materials research, for example, intercalated compounds of MoO_3 have been synthesized via various chemical routes,[1,2,7,12] which include thermal intercalation of amines and aniline,[2] spin-coating of $MoO_3 \cdot nH_2O$ electrochromic films,[7] electrochemical synthesis of $K_{0.3}MoO_3$, and cation exchange to form $MoO_3^{x-}(Na^+)_x$.[1,2] On the other hand, MoO_3-based metal oxides that form the backbone of MoO_3 derivative materials have been synthesized by different thermal processes. In particular, solid-state reactions for ceramic or catalytic materials have been conducted at medium-range temperatures of a few hundred °C,[4,8,10] while melt syntheses at a temperature from a few hundred °C to more than 1060 °C.[3,5]

Regarding the MoO_3 in the above compound syntheses, there are two material issues needed to be addressed. The first question here concerns how to fabricate stoichiometric MoO_3 with a defined crystallographic structure, as many intercalated compounds are prepared from this material precursor. Due to the high volatility of MoO_3,[4] the chemical composition and stoichiometry of the thermally synthesized materials often depart from the originally desired ones. Therefore the second question one may have is what are the vaporization and condensation behaviors of MoO_3 in a thermal process of material synthesis.

Over past 10 years, thin films and microcrystals of MoO_3 have been prepared by a number of ways.[13−19] In particular, the high volatility of MoO_3 has been utilized in thin-film growth by the vacuum evaporation method.[13] Other techniques, such as rf sputtering and electron beam techniques and chemical vapor deposition, have also been explored in MoO_3 thin-film fabrication.[14−17] In recent years, flash evaporation and molybdenum metal oxidation have been studied for the processing of MoO_3 thin films and microcrystals, respectively.[18,19] It

* Corresponding author. Tel: +65 772 2896. Telefax: +65 779 1936. E-mail: chezhc@leonis.nus.sg.

(1) Thorne, R. E. *Phys. Today* **1996**, *49*(5), 42.
(2) Tagaya, H.; Ara, K.; Kadokawa, J.-I.; Karasu, M.; Chiba, K. *J. Mater. Chem.* **1994**, *4*, 551.
(3) Sekiya, T.; Mochida, N.; Ogawa, S. *J. Non-Cryst. Solids* **1995**, *185*, 135.
(4) Zeng, H. C. *J. Mater. Res.* **1996**, *11*, 703.
(5) Zeng, H. C. *J. Cryst. Growth* **1996**, *160*, 119.
(6) Colton, B. J.; Guzman, A. M.; Rabalais, J. W. *J. Appl. Phys.* **1978**, *49*, 409.
(7) Hinokuma, K.; Kishimoto, A.; Kudo, T. *J. Electrochem. Soc.* **1994**, *141*, 876.
(8) Sabu, K. R.; Rao, K. V.; Nair, C. G. R. *Indian J. Chem.* **1994**, *33*B, 1053.
(9) Zhang, C.-M.; Chen, S.-Y.; Yang, Z.-P.; Peng, S.-Y. In *Sol−Gel Processing and Applications*; Attia, Y. A., Ed.; Plenum Press: New York, 1994; p 379.
(10) Hayashi, H.; Sugiyama, S.; Masaoka, N.; Shigemoto, N. *Ind. Eng. Chem. Res.* **1995**, *34*, 137.
(11) Fournier, M.; Aouissi, A.; Rocchiccioli-Deltcheff, C. *J. Chem. Soc., Chem. Commun.* **1994**, 307.
(12) Benard, P.; Seguin, L.; Louer, D.; Figlarz, M. *J. Solid State Chem.* **1994**, *108*, 170.
(13) Anwar, M.; Hogarth, C. A. *Int. J. Electron.* **1989**, *66*, 901.
(14) Ohfuji, S. *Thin Solid Films* **1984**, *115*, 299.
(15) Ohtsuka, H.; Yamaki, J. *Solid State Ionics* **1989**, *35*, 201.
(16) Arnoldussen, T. C. *J. Electrochem. Soc.* **1976**, *123*, 527.
(17) Donnadieu, A.; Davazoglou, D.; Abdellaoui, A. *Thin Solid Films* **1988**, *164*, 333.
(18) Julien, C.; Khelfa, A.; Hussain, O. M.; Nazri, G. A. *J. Cryst. Growth* **1995**, *156*, 235.
(19) Kim, H.-M.; Fukumoto, T.; Hayashi, S.; Yamamoto, K. *J. Phys. Soc. Jpn.* **1994**, *63*, 2194.

S0897-4756(97)00345-1 CCC: $15.00
Published on Web 03/06/1998

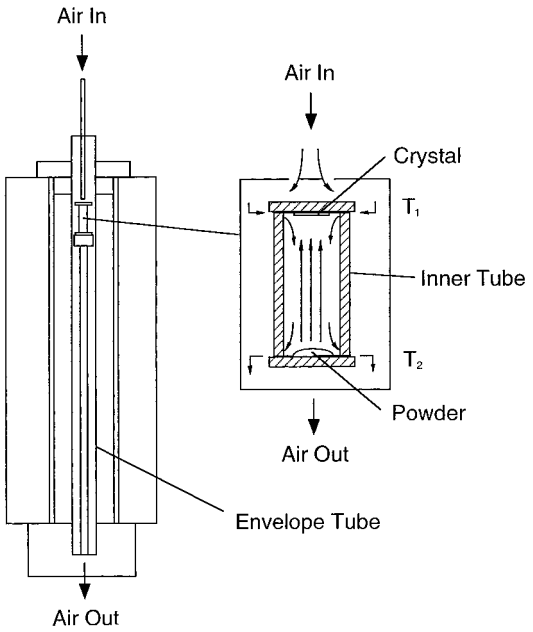

Figure 1. Kinetic study setup. The insert indicates the structure of condensation compartment, noting that purified air enters the top plate and flows down to the bottom.

is noted that in most cases either a low-pressure or vacuum condition is required. Thus, from both technological and fundamental viewpoints, new processes with less-demanding fabrication conditions are urgently needed.

In conjunction with a systematic vapor-phase growth of orthorhombic MoO_3 crystals, we establish in this work a new growth kinetic approach to study the vaporization−condensation of highly volatile metal oxides. The growth experiments were conducted under normal atmospheric pressure with air as background gas to ensure a sufficient O_2 supply to the growth.

Experimental Section

The vapor-phase growth of crystalline MoO_3 was conducted in a vertical Carbolite electric furnace. The furnace structure and experimental setup are depicted in Figure 1. The growth chamber is comprised of an inner quartz tube and two pieces of plates of the same material. To control the growth atmosphere, the above chamber tube was further enveloped in another quartz tube with a greater diameter. The growth process can be briefly summarized as follows. The nutrient material of as-received MoO_3 powder (50.0 mg in each run) was loaded on the bottom plate, which was located in the heating zone of furnace. The top quartz plate serving as growth zone was distanced from the MoO_3 nutrient by the inner tube. Temperatures of source zone and growth zone were measured with a K-type thermocouple. In a typical experiment, the growth atmosphere (purified cylinder air) was introduced from the top of envelope tube to the upper quartz plate at a flow rate of 15.0 L/h. The source nutrient MoO_3 was maintained at the constant temperature of 677−702 °C for various time lengths (Table 1). Crystalline MoO_3 were grown on the top plate where the temperature gradient was about −(10.7−12.5) °C/cm from the bottom. It should be mentioned that under these experimental conditions, no condensation of MoO_3 was observed on the wall of the inner tube. Other growth parameters are also listed in Table 1 for further reference.

To obtain kinetic growth data, amounts of residual source MoO_3 and crystals grown were determined by measuring the weight difference of the respective quartz plates before and after each experiment. The crystallographic structure of

Table 1. Growth Parameters for the Vapor Phase Grown MoO_3 Crystals

growth atmosphere	air (purified)
air-flow rate	15.0 L/h
growth temp (T_1)	642, 650, 660, 672 °C (top plate)
nutrient temp (T_2)	677, 684, 695, 702 °C (bottom plate)
temp gradient	−12.5, −12.4, −12.5, −10.7 °C/cm (above the nutrient)
heating rate	10.0 °C/min
cooling rate	10.0 °C/min
growth time	2−16 h
growth facility material	quartz
quartz-plate dimension	20 × 20 × 3 (length × length × thickness)
chamber tube volume	12 mm × 28 mm × 1.5 mm (diameter × height × thickness)
envelope tube volume	30 mm × 1300 mm × 2.5 mm (diameter × height × thickness)

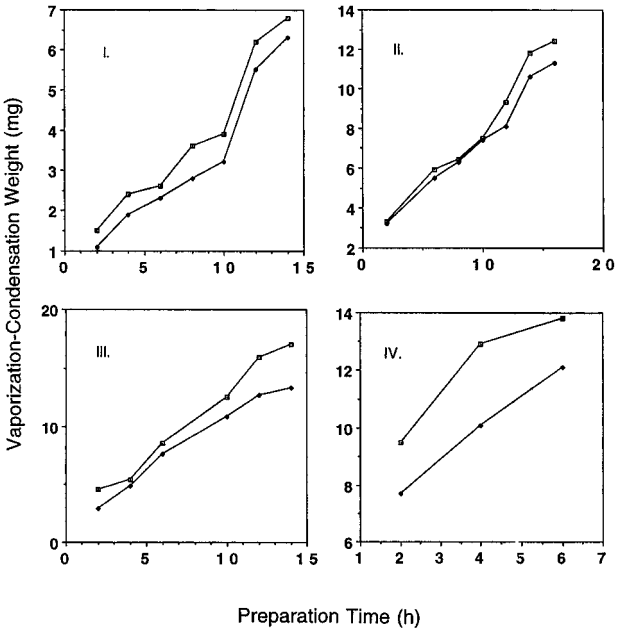

Figure 2. Weight data of vaporization (upper curve) and condensation (lower curve): (i) $T_1 = 642$ °C and $T_2 = 677$ °C, (ii) $T_1 = 650$ °C and $T_2 = 684$ °C, (iii) $T_1 = 660$ °C and $T_2 = 695$ °C, and (iv) $T_1 = 672$ °C and $T_2 = 702$ °C; the air-flow rate was fixed at 15 L/h.

grown MoO_3 crystals was investigated with powder X-ray diffraction (XRD, Philips PW 1729) and KBr-pellet technique of Fourier transform infrared spectroscopy (FTIR, Shimadzu FTIR-8001). The morphology of the crystals was examined with an optical microscope (Olympus BH-2), and the major growth planes of the crystal was determined by measuring interplanar angles.

Results and Discussion

Vaporization and Condensation. In Figure 2, kinetic data of four series (I−IV) of grown MoO_3 crystals versus growth time are displayed. As can be seen, most of these experiments give a close relationship between vaporization and condensation, except the series IV and two cases in series III (at 12 and 14 h) which show a greater difference between the powder loss and crystal gain. These results clearly indicate that with the current experimental setup, the growths were conducted at near steady state, i.e., the evaporation rate of the source MoO_3 almost equals the condensation.

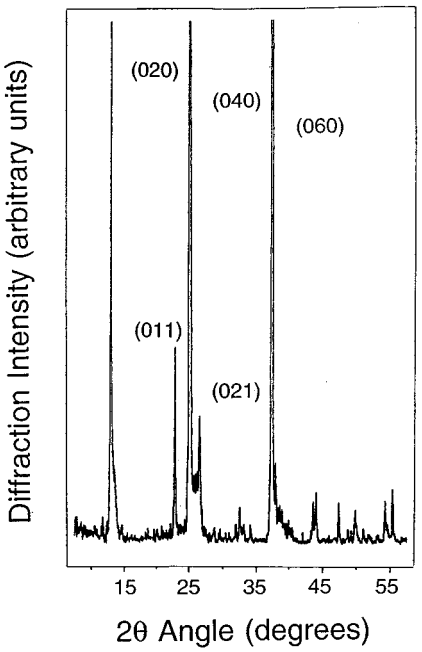

Figure 3. Representative XRD spectrum for the orthorhombic MoO_3 samples.

It should be mentioned that under the current experimental arrangement, gaseous species can travel freely between the growth chamber and envelope tube due to the interstitial space between the quartz plates and chamber tube. It had been reported that the low oxidation state Mo^{5+} and oxygen defects are responsible for the alternation of intrinsic conductivity of MoO_3.[18,20−22] One of the advantages of this experimental setup is that it allows vaporized species to interact with O_2 in a growth ambient, as the rising vapor (the bottom plate is hotter than the top one) countermeets with the O_2 entering from the top plate-tube space. This maximum interaction between the ambient air and source vapor is important to ensure the following chemical equilibrium shifted to the left:

$$2MoO_3 \rightleftharpoons 2MoO_{3-x} + xO_2 \qquad (1)$$

The oxygen exchange between the lattice and ambient species has been investigated with the isotope ($^{18}O_2$) labeling technique and Raman spectroscopy, which shows that gaseous O_2 is able to incorporate into oxygen-deficient MoO_3.[22] Furthermore, unlike the vacuum growths,[13−17] the current growth system can be operated at normal pressure (1 atm) for the growth process. The experimental requirements have thus been simplified.

As revealed in Figures 3 and 4 respectively for XRD and morphological studies, it is found that the grown crystals are largely in orthorhombic structure (α-MoO_3),[23] which is the most thermodynamically stable polymorphic form. The crystals are platelike rectangles with their {010} parallel to the top quartz plate.

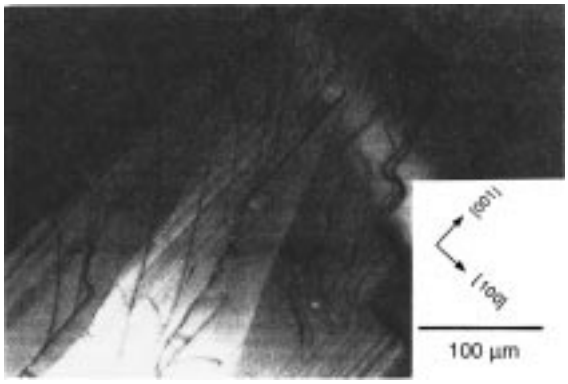

Figure 4. Micrograph for the crystal morphology of orthorhombic MoO_3 samples.

Table 2. Vapor Pressures and Growth Rates of MoO_3 in the Series I−IV

series	T_1 (°C)	T_2 (°C)	P_1 (Pa)	P_2 (Pa)	ΔP (Pa)	R_E (mg/h)	ln (ΔP)	ln R_E
I	642	677	4.77	18.40	13.63	0.25	2.61	−1.3863
II	650	684	6.56	23.81	17.25	0.51	2.85	−0.6733
III	660	695	9.69	35.39	25.70	1.00	3.25	0
IV	672	702	15.27	45.31	30.04	1.10	3.40	0.0953

Apparently the growth is singular on the {010} crystallographic planes. It is also observable that terraces, ledges, and kinks on these slowest growing planes are advancing in the major growth directions ⟨001⟩.

Empirical Growth Rate Estimation. In the current vapor-phase growth, the degree of supersaturation can be related to the difference of saturated vapor pressures between the bottom and top plates as $\Delta P/P_1 = (P_2 - P_1)/P_1$.[24] From the data listed in Tables 1 and 2, it is recognized that ΔP would be small during the growth since T_2 is not far from T_1. Furthermore, fluid mixing of the vapor is enhanced by the counterstream of air; transport processes are unlikely to be rate-limiting. Due to these, the rate law of the current growths can be described empirically by

$$R_E = k\Delta P^n \qquad (2.1)$$

$$\ln R_E = \ln k + n \ln(\Delta P) \qquad (2.2)$$

where k is a rate constant and $3n$ is an integer within $1 \le 3n \le 12$.[24] If transport processes interfere with the growth, the experimental value of n is usually nearer to unity in this empirical rate expression.[24] It should be pointed out that in order to use this equation, experimental kinetic data must be linear with respect to time since the right-hand term of eq 2.1 is a constant for a particular temperature setting.

To calculate ΔP and thus n, the following correlation of MoO_3 vapor pressure (in atm) to temperature (in K) can be used:[25]

$$\log P = -15110T^{-1} + 1.46 \log T - 1.32 \times 10^{-3}T + 9.071 \qquad (3)$$

Using the above equation, pressure differences ΔP are calculated for the growth series I−IV, which are reported in Table 2. On the basis of their linear portions

(20) Anwar, M.; Hogarth, C. A.; Lott, K. A. K. *J. Mater. Sci.* **1989**, *24*, 1660.
(21) Anwar, M.; Hogarth, C. A.; Bulpett, R. *J. Mater. Sci.* **1989**, *24*, 3087.
(22) Mestl, G.; Ruiz, P.; Delmon, B.; Knozinger, H. *J. Phys. Chem.* **1994**, *98*, 11269.
(23) Chippindale, A. M.; Cheetham, A. K. In *Molybdenum: An Outline of Its Chemistry and Uses*; Braithwaite, E. R., Haber, J., Eds.; Elsevier Science: Amsterdam, 1994; Chapter 3, p 146.
(24) Brice, J. C. *Crystal Growth Processes*; Halsted Press: New York, 1986; Chapter 9, p 212.

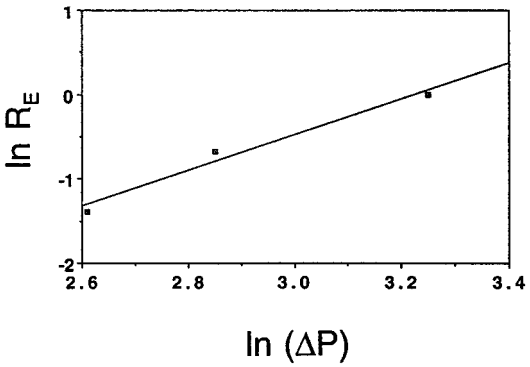

Figure 5. ln R_E versus ln(ΔP) plot based on the data of series I−III.

of kinetic data (Figure 2), constant rates for the growth series I−IV are also obtained respectively in Table 2. By plotting ln R_E versus ln(ΔP) of series I−III in Figure 5, the slope and intercept of eq 2.2 are calculated to be $n = 2.07$ and $\ln k = -6.7275$, respectively, and the empirical rate law for the three series of growths can thus be written as

$$R_E = 1.20 \times 10^{-3} \Delta P^{2.07} \tag{4}$$

Noting that $3n \approx 6$ is well in the middle of the range $1 \leq 3n \leq 12$, the transport problem is thus insignificant during the growth.[24] It is important to realize that when the experimental temperature is too high, such as in the series IV, the accuracy of the growth rate predicted by the above equation will decrease. For example, the calculated rate using eq 4 is 1.4 mg/h for the series IV, which is apparently in the high side compared to the experimental one, 1.1 mg/h, in Table 2. This discrepancy will be discussed shortly.

Langmuir−Hinshelwood Kinetic Description. The above rate investigation has shown us good correlation between the experimental rate data and model prediction for the linear portions of the series I−III. Nevertheless, to address the nonlinear part, such as in the case of series I (Figure 2, 12−14 h), and the gap between vaporization-condensation shown in series III (Figure 2, 12−14 h) and IV, better kinetic models need to be investigated.

Regarding the growths in current work, it should be realized that there are at least two stages of growth in each experiment. The first one, during the induction period, is the heterogeneous growth (or nucleation) of MoO_3 on a quartz plate. Stage two is then followed, which is a steady-state homogeneous growth of MoO_3 on MoO_3 covered quartz plate. On the basis of the kinetic data shown in Figure 2, it can be deduced that the stage-one growth had been completed within 2 h in all cases. Since the grown crystals have growth planes which contain terraces, ledges, and kinks, it is believed that the second-stage growth (and/or later stages) is a singular type, i.e., layer-by-layer growth (Frank−Van der Merwe mode). For this reason, the Langmuir−Hinshelwood kinetic theory[26] will be applied to the growths after the induction period:

(25) Killeffer, D. H.; Arthur, L. *Molybdenum Compounds, Their Chemistry and Technology*; Interscience: New York, 1952; p 31.

(26) Zangwill, A. *Physics at Surfaces*; Cambridge University Press: Cambridge, 1990; Chapter 15, p 400.

$$\text{Step 1} \qquad M(s) \rightarrow M(g) \tag{5.1}$$

$$\text{Step 2} \qquad M(g) + S \rightleftharpoons M{\cdot}S \tag{5.2}$$

$$\text{Step 3} \qquad M{\cdot}S \rightarrow M(c) + S \tag{5.3}$$

Related to the experimental setup, in Figure 6, solid-phase MoO_3, M(s), is vaporized from the bottom plate in step 1 to become vapor M(g) which contains cyclic Mo_3O_9, Mo_4O_{12}, and Mo_5O_{15} gaseous molecules.[26] The second step represents the adsorption of the vapor species M(g) onto a vacant site S, to form the adspecies M·S. However, an adspecies can also desorb back to the vapor phase in a reverse process. Since the grown {010} surfaces are rather smooth, migration of an adspecies on the terrace should be relatively easy. Therefore step 3 is thought to be the one responsible for the actual crystal growth—incorporation of adspecies into an energetically favorable site of a ledge or kink. The M(c) refers to the newly formed crystalline MoO_3, which is now part of the entire lattice.

According to step 2, the net rate of vapor MoO_3 transfer to the surface can be written as

$$R_N = k_2 C_{M(g)} C_S - k_{-2} C_{M\cdot S} = k_2 (C_{M(g)} C_S - C_{M\cdot S}/K_M) \tag{6.1}$$

where k_2 and k_{-2} are adsorption and desorption rate constants ($K_M = k_2/k_{-2}$); $C_{M(g)}$, C_S and $C_{M\cdot S}$ are the volumetric concentration of MoO_3 vapor, surface concentration of vacant sites, and surface concentration of adspecies, respectively. The crystal growth rate can be calculated from the rate law based on the rate-limiting step 3:

$$R_G = k_3 C_{M\cdot S} \tag{6.2}$$

where k_3 is rate constant of this M·S incorporation process. Applying the basis for the pseudo-steady-state growth approximation ($R_N/k_2 \approx 0$), eq 6.1 gives

$$C_{M\cdot S} = K_M C_{M(g)} C_S \tag{6.3}$$

Substituting eq 6.3 into eq 6.2, the growth rate is

$$R_G = k_3 K_M C_{M(g)} C_S \tag{6.4}$$

If C_T represents total sites per unit of surface area which consist of vacant sites (C_S) and adsorbed sites ($C_{M\cdot S}$), eq 6.4 can be rewritten as

$$R_G = k_3 K_M C_{M(g)} C_T / (K_M C_{M(g)} + 1) \tag{6.5}$$

Equation 6.5 gives a constant growth rate R_G at a studied temperature, if the total surface site concentration, $C_T = C_S + C_{M\cdot S}$, is constant. Similar to the R_E obtained by the empirical rate law, eq 6.5 describes nicely the linear portions of growth (stage two, Figure 2). Since the remaining terms in eq 6.5 are constants when the temperature is fixed, in the following we shall examine only the effect of C_T on the growth rate R_G to explain the nonlinear growths (or staged growths) observed in the experiments with longer growth times (12−14 h, Figure 2).

In Figure 7, some schematic representations to explain these staged condensations will be further addressed. When they were prepared at low temperature

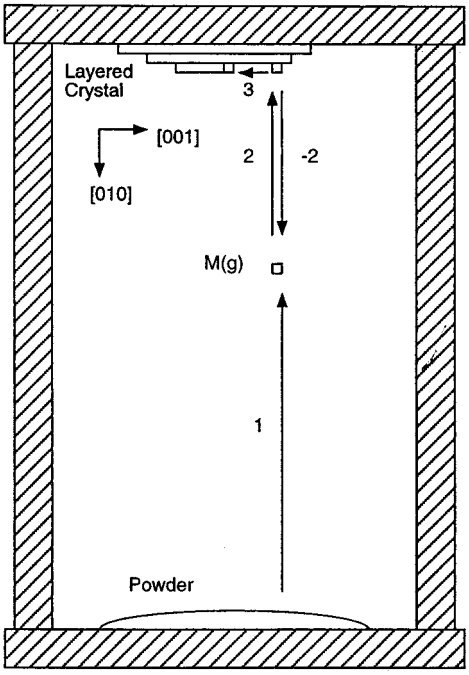

Figure 6. Illustration of proposed growth mechanism for eqs 5.1−5.3.

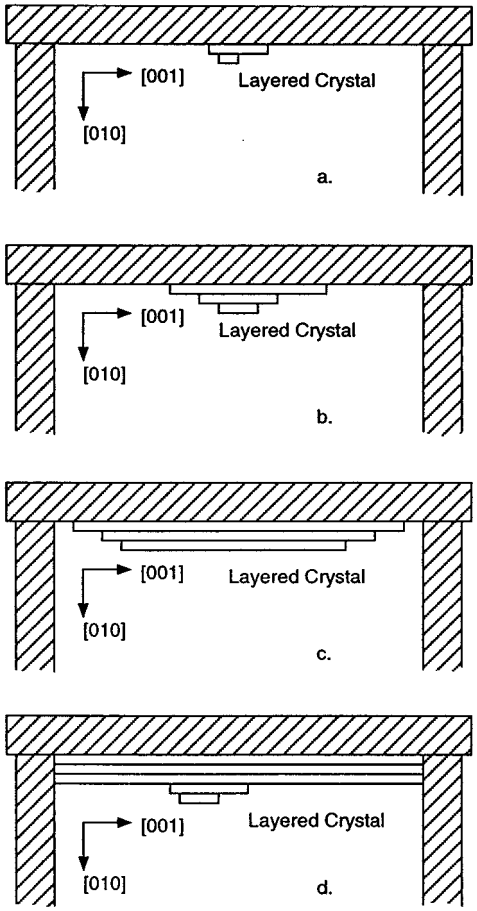

Figure 7. Schematic representations of growth process in various growth stages; only one crystal is illustrated.

(series I), MoO_3 crystals are mainly located in the center of the upper plate with appearance of sheetlike ribbons normal to ⟨010⟩. These crystals have a similar dimensional ratio of ⟨001⟩:⟨100⟩ which is much greater than 1. This in fact indicates that the growth is a "free" lateral growth in both ⟨001⟩ and ⟨100⟩ directions, although ⟨001⟩ growth is faster than ⟨100⟩ (stage a, Figure 7). The free lateral expansion along these directions would result in an increase in surface area of {010} planes and steps, which in turn implies an increase of total surface sites C_T after the crystal reaches certain critical dimensions (stage b, Figure 7). According to eq 6.5, an increase in C_T will result in a rise of growth rate. This can explain nicely why a sudden weight increase in the last two data of the series I, i.e., from stage a to stage b (Figure 7).

On the contrary, when the crystal was grown at a higher temperature (series III) with long growth time (12−14 h, Table 2), it is found that the crystals are cross-linked and crowded; they are confined within the circumference of the chamber tube (stage c, Figure 7). Apparently, the MoO_3 crystals in such a case are much thicker in ⟨010⟩ directions (stage d, Figure 7). On the basis of this observation, it can be concluded that after a "not-so-free" lateral growth in the ⟨001⟩ and ⟨100⟩ directions, the growth has been switched to the {010} planar growth. The speed of this is certainly lower compared with the "free" growths on {001} and {100} planes. With high mobility of adspecies at this temperature (660 versus 642 °C, Table 2), it would not be surprising that the vacant site concentration (C_S) and thus C_T will be reduced when the crystals are forced to grow on {010} surfaces (stage d, Figure 7), as observed in the departure of vaporization−condensation data in Figure 2 (series III). A similar explanation can be given to the series IV, the cases of the fastest growth. It is observed that the growth of this type is mainly in ⟨010⟩ directions for a longer processing time (6 h). That is why the kinetic data of the series IV are not being used in the n and k calculations, as it departs markedly from the linearity of ln R_E versus ln(ΔP) plot (see also Table 2).

As for the growth series II, one can view it as an intermediate case between the series I and III. The linear correlation of vaporization−condensation indicates a steady-state lateral growth along the ⟨001⟩ and ⟨100⟩ directions (i.e., from stage b to c, Figure 7). This type of growth seems to have optimum growth conditions with this method, as the condensation synchronizes with vaporization throughout the experiments (2−16 h).

Thermodynamic Consideration. In the previous section, it was found that α-MoO_3 crystals prefer to grow along ⟨001⟩ and ⟨100⟩ directions, resulting in ⟨010⟩ oriented sheets parallel to the quartz plate. To have a better understanding of this, thermodynamic factors related to the growths need to be further considered.

It is essential for the source MoO_3 powder to vaporize before an actual growth can be commenced. Concerning such a vaporization process, the change in free energy for the source MoO_3 can be written as

$$\Delta G_{s\to g} = \Delta H_{s\to g} - T_2 \Delta S_{s\to g} \qquad (7.1)$$

where $\Delta G_{s\to g}$ is the free energy difference between molecules in the solid phase and in vapor, T_2 is the sublimation (or vaporization) temperature, and $\Delta H_{s\to g}$ and $\Delta S_{s\to g}$ are the phase transition latent heat and the entropy related to process, respectively. However, under equilibrium condition, $T_2 = T_1$ (bottom and top

Table 3. $\Delta G_{s\to g}$ and $\Delta G_{g\to c}$ Data Calculated for MoO_3 Vaporization and Crystallization in Series I−IV Using Eqs 7.4 and 7.5, Respectively

series	T_1 (K)	T_2 (K)	ΔT (K)	$\Delta G_{s\to g}$ (kJ/mol)	P_1 (Pa)	P_2 (Pa)	P_2/P_1	$\Delta G_{g\to c}$ (kJ/mol)
I	915	950	−35	−10.6	4.77	18.40	3.86	−10.7
II	923	957	−34	−10.3	6.56	23.81	3.63	−10.3
III	933	968	−35	−10.4	9.69	35.39	3.65	−10.4
IV	945	975	−30	−8.8	15.27	45.31	2.97	−8.8

plates both are set at an identical temperature), one would expect there is no net vaporization from the bottom plate MoO_3, and eq 7.1 becomes

$$\Delta G_{s\to g} = 0 = \Delta H_{s\to g} - T_1 \Delta S_{s\to g} \tag{7.2}$$

From eq 7.2, we have

$$\Delta S_{s\to g} = \Delta H_{s\to g}/T_1 \tag{7.3}$$

Thus, eq 7.1 can be rewritten as

$$\begin{aligned} \Delta G_{s\to g} &= \Delta H_{s\to g} - T_2 \Delta S_{s\to g} \\ &= \Delta H_{s\to g} - T_2 \Delta H_{s\to g}/T_1 \\ &= \Delta H_{s\to g} \Delta T/T_1 \end{aligned} \tag{7.4}$$

where $\Delta T = T_1 - T_2$, assuming $\Delta H_{s\to g}$ and $\Delta S_{s\to g}$ are invariant over the narrow operating temperature range. Using eq 3 and the Clausius−Clapeyron equation,[27] $\Delta H_{s\to g}$ is determined to be 278.16 kJ/mol over the temperature range 923−973 K. Calculated $\Delta G_{s\to g}$ data for the series I−IV are listed in Table 3. Referred to eq 7.4, it is recognized that, with the current setup, $\Delta H_{s\to g}$ is a constant within the temperature range studied and $\Delta G_{s\to g}$ would depend mainly on $\Delta T/T_1$. Apparently, experiments at higher temperature iron out the temperature difference between the top and bottom plates (ΔT). With the current settings, lower T_1 promotes MoO_3 vaporization from the source (at T_2), which is true in the data calculated for most series studied. The small rise of $\Delta G_{s\to g}$ in the series III should be attributable to a less-accurate temperature measurement for this series, since its ΔT (=−35) differs from the general trend in Table 3.

Viewing the same question (driving force) from another angle, one may wish to see free energy changes for the source MoO_3 vapor being incorporated into crystal lattice, i.e., a process of changing high saturated pressure P_2 on the source powder to low saturated pressure P_1 on the crystal surfaces. This can be done by looking at the free energy change in vapor-phase growth

$$\Delta G_{g\to c} = -RT_2 \ln(P_2/P_1) \tag{7.5}$$

where R is the universal gas constant, noting that eq 7.5 is another version of eq 7.4 which can be converted by the Clausius−Clapeyron equation.[27] Obviously, a higher P_2/P_1 ratio would give a larger driving force for crystallization. In other words, the crystallization would occur at the place with maximum supersaturation $\Delta P/P_1 = (P_2 - P_1)/P_1$. This explains why the growths are parallel to the top quartz plate to keep the farthest distance from the vapor source and thus the smallest P_1. As a result, the downward growth into the chamber tube becomes difficult. On the basis of the above equation, the calculated $\Delta G_{g\to c}$ are also reported in Table 3. Again, at a lower temperature, crystallization driving force of series I is the greatest among the four due to a high P_2/P_1 ratio, while it is the smallest for the series IV. Both $\Delta G_{s\to g}$ and $\Delta G_{g\to c}$ values are very similar, since they facet the same issue from different angles. The low yield observed in the series IV can now be further addressed. In view of the fact that $\Delta T/T_1$ or $\Delta P/P_1$ is small in this case, it can be understood that evaporation is easier than the condensation in a higher temperature operation.

From the above two thermodynamic viewpoints, the kinetic behaviors observed in the previous sections can now be better understood. To optimize the growth parameters, one has to strike a balance between kinetic and thermodynamic considerations. In particular, when conducting a kinetic growth study of MoO_3, one has to give considerations both to the intrinsic thermodynamic factors of crystal such as actual growth orientation and to the thermodynamic driving force due to experimental conditions.

Conclusions

In summary, a simple kinetic method has been demonstrated in this paper for highly volatile oxide compounds. The method also ensures sufficient oxygen supply to the condensation process to maintain the correct stoichiometry of the compound. In this work, the vaporization and condensation of orthorhombic molybdenum trioxide (MoO_3) has been investigated. The empirical growth rate of the MoO_3 crystals obtained is $R_E = 1.20 \times 10^{-3} \Delta P^{2.07}$ at 642−660 °C, where ΔP is the partial pressure difference of MoO_3 between the source and condensed crystals. On the basis of the observed layered structure of MoO_3 crystals, a Langmuir−Hinshelwood kinetic description for the MoO_3 condensation has been proposed to address different slopes observed in the weight data. The driving force of the condensation growth has been further addressed with respect to the process parameters such as partial pressure difference and temperature gradient. For the MoO_3 partial pressure ratios of 3.86−2.97 between the source and condensed MoO_3, free energy changes estimated for the condensation growth are in the range of −10.7 to −8.8 kJ/mol.

Acknowledgment. The authors gratefully acknowledge the research fundings supported by the Ministry of Education and National Science and Technology Board of Singapore.

CM970345P

(27) Alberty, R. A. *Physical Chemistry*; Wiley: New York, 1987; Chapter 6, p 187.